Fluorescence correlation spectroscopy on electron transfer reactions : probing inter- and intramolecular redox processes

Sen, S.

Chapter 2

Calibration of experimental setup, bimolecular reactions and photoinduced electron-transfer reactions

Abstract

The calibration of the instrumental setup required for fluorescence correlation measurements is reported. Calibration was performed using a commercially available organic dye ATTO655 and recording its fluorescence intensities (autocorrelation functions) over time having different concentrations. The instrumental factor "*k*" obtained through the calibration measurements has been used for the fitting of the autocorrelation curves (ACF) of labeled Zinc and Copper azurin samples in Chapter 3, 4 and 5. This chapter also includes a general discussion of bimolecular interactions and photoinduced electron transfer reactions in proteins.

2.1 *Introduction*

When diffusion was first analyzed by Stokes and Einstein(*1*)(*2*)(*3*), its importance soon gained recognition in the scientific world and the concept of diffusional motion found use in the fields of fluid mechanics, biophysics, soft-condensed-matter physics. Since then, a variety of experimental methods has been developed to monitor particles in solution. Fluorescence correlation spectroscopy (FCS) was introduced in the 1970s as a technique to study diffusion(*4*). In the beginning, the main drawback with this method was the large observation volume and low signal to noise ratio. Later on, with the implementation of confocal microscopy and advanced hard- and software, it became a powerful technique for biological applications(*5*)(*6*)(*7*)(*8*)(*9*). In recent years, this technique has been developed further, and FCS became widely applicable from biology and chemistry *in vitro* to the study of molecular motions inside the living cells.

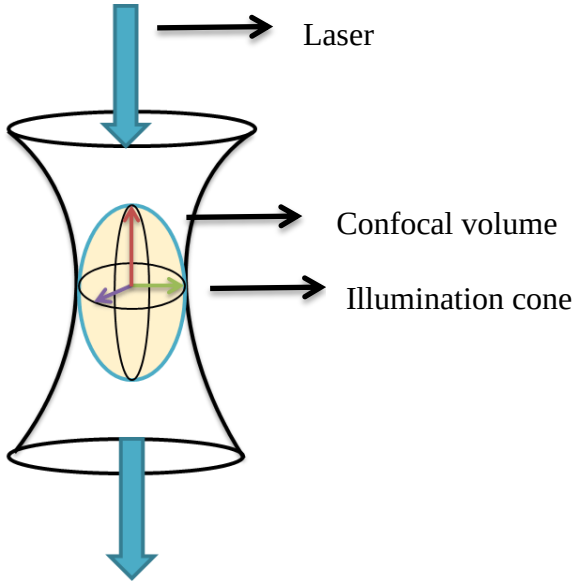

Figure 2.1: *A cartoon depicting the confocal volume and the illumination cone generated by a tightly focused laser in solution. x-, y- and z-axis of the confocal volume have been represented by green, violet and red arrows. A three-dimensional parameter k for the instrument is expressed as the ratio of the length of z-axis to that of the axes in the xy-plane.*

As discussed in the previous chapter, the principle of FCS is to measure fluorescence intensity fluctuations caused by labeled molecules diffusing in and out of the confocal volume of a fluorescence microscope. A schematic diagram of the confocal volume is displayed in Figure 2.1. Fluorescence fluctuations are correlated over time, and the autocorrelation function *G(t)* is

generated. *G(t)* decays as the molecules diffuse out of the confocal volume with a characteristic correlation time τ_D, which is related to the diffusion coefficient *D* of the diffusing molecules. Accurate evaluation of the confocal volume is needed for the correct interpretation of experimental data and the design of an appropriate diffusion model. The three-dimensional parameters *k* and r_0 (*vide infra*) describe the geometry of the volume as displayed in Figure 2.1. In a calibration procedure to be described here, a reference dye is used to measure those parameters(*10*)(*11*)(*12*).

ATTO655 is a dye well-suited to calibrate a confocal microscope. It has a strong absorption, high fluorescence quantum yield and high thermal and photostability. It also has good water solubility. The fluorescence excitation range of ATTO655 dye is from 640 - 660 nm. The diffusion coefficient of ATTO655 NHS ester dye has been measured to be 425±6 $\mu m^2/s$ at 295 K(*11*).

As the diffusion motion of dye molecules is influenced by the properties of the liquid in which the dyes are dissolved, we can observe the reaction dynamics on a time scale between picoseconds and milliseconds depending on the solvent by FCS. The lower limit is defined by the instrument response function while the residence time of the labeled molecules in the confocal volume controls the upper limit. This residence time can be varied by changing the viscosity of the solution, or by linking the molecules to bigger, and thereby slower diffusing particles. In the present thesis, sucrose has been used to increase the viscosity of the medium. In our experiments, the solution conditions were varied from pure water (viscosity ~1 cP) to 57.0% (w/w) sucrose (viscosity ~37.5 cP) at room temperature (22 ºC). This has allowed investigation of inter- as well as intra-molecular dynamics of the azurin-dye conjugate.

We calibrated our FCS setup using pure buffer and a 57.0% (w/w) sucrose solution containing different ATTO655 dye concentrations. The main goal of this work was to precisely determine the three-dimensional parameters (*k* and r_0) of the experimental setup. The results were used in our FCS measurements discussed in the next chapters.

2.2 *Materials and Methods*

2.2.1 *Reagents and Samples*

Unless stated otherwise, all the reagents were purchased from Sigma-Aldrich (Sigma-Aldrich Corp., St. Louis, USA) and used as received. The fluorescent label ATTO655 N-

hydroxysuccinimidyl ester (NHS-ester: Product no. AD-655-31) was purchased from ATTO-TEC GmbH (Siegen, Germany) as a powder and dissolved in water-free DMSO before use, as suggested by the supplier. Sucrose was purchased from Sigma-Aldrich (Product no. 84100-microbiology grade). Chemical structure of ATTO655 has been shown in Fig. 1.4A in Chapter 1. It has been reported that ATTO655 has a tendency to dimerize which could result in a reduction of the diffusion coefficient at high concentrations(*13*). Hence, most of the diffusion measurements were performed on samples in the concentration ranges of from pM to nM. Samples for the FCS calibration measurements with different ATTO655 concentrations (100 pM to 10 nM) were prepared by dissolving small amounts of the dye in 20 mM HEPES pH 7.0 buffer or in 57% (w/w) sucrose containing 0.05% Tween-20 (a detergent polysorbate) to prevent any surface adhesion or aggregation.

2.2.2 *Preparation of sucrose solution*

A 75% (w/v) stock solution of sucrose was prepared by adding 10 ml of a 500 mM HEPES pH 7.0 buffer solution to 37.5 g of high purity (purity >99.5%) D(+)-saccharose powder. The volume was adjusted to 50 ml by adding Milli-Q water or buffer. The solution was thoroughly sonicated to achieve complete dissolution of the sucrose and degassed to avoid the presence of air bubbles. The precise concentration of the solution was checked by measuring the refractive index n_r, which was determined at 22ºC with a Zeiss Abbe refractometer (Carl Zeiss, Germany). The refractive index of several preparations of the stock solution was found to be 1.445 (±0.002) corresponding with a content of 61.4% sucrose (w/w) and a viscosity of 75 cP(*14*). Table 2.1 shows the variation of refractive indexes of the aqueous sucrose solutions prepared for FCS measurements as a function of sucrose concentration.

Amount of sucrose stock solution (µl)	Amount of Buffer (µl)	Refractive Index (n_r)(a)	Composition (%w/w)(b)	Viscosity (cP) (c)
400	0	1.445±0.002	61.4	75.0
372	28	1.435±0.002	57.0	37.5
320	80	1.415±0.002	47.6	12.1
267	133	1.393±0.002	36.5	4.90
187	213	1.382±0.002	30.5	3.25
91	309	1.367±0.002	21.9	2.12
42	358	1.347±0.002	9.4	1.30
0	400	1.330±0.002	0	1.00

Table 2.1: *Viscosity and refractive indexes for the sucrose solutions. (a) Data obtained using Zeiss Abbe refractometer (Carl Zeiss, Germany), (b) Composition of the sucrose solutions according to the tables in the CRC Handbook of Chemistry and Physics relating composition to refractive index (check ref(16)), (c) Viscosities of the sucrose solutions according to the tables in the CRC Handbook of Chemistry and Physics relating composition to viscosity (ref(16) for details).*

2.2.3 *Sample preparation for FCS experiments*

For each measurement, a fresh sample solution was prepared by mixing 372 µl of the sucrose stock solution (75 % w/v) with 4 µl of bovine serum albumin (BSA) stock solution (10 mg/ml), 4 µl of a 100 nM azurin stock solution and between 10 and 20 µl of 2 or 20 mM freshly prepared stock solutions of ascorbate or hexacyanoferrate(II) or (III). The sample was adjusted to 400 µl by admixture (≤ 20 µl) of 100 mM HEPES buffer, pH 7.0. The precise concentration of the sample solution was checked by measuring the refractive index n_r at 22ºC with a Zeiss Abbe refractometer and the sucrose content of the samples was found to be 57.0% (w/w) (i.e. 70% w/v) , corresponding to a viscosity of 37.5 cP at 22^0C. The final sample concentration of labeled azurin was around 0.4-0.8 nM (for azurin expression and purification, see Chapter 3 for details). For calibration measurements of the instrument, samples were prepared containing only ATTO655 dye (no azurin) without redox agents.

2.2.4 *FCS setup*

The FCS calibration measurements were carried out at room temperature on a home-built confocal setup (Fig. 2.2B) equipped with an Axiovert 100 inverted microscope (Carl Zeiss, Germany) and a high numerical aperture (NA) water immersion objective (60x water, NA 1.2,

Olympus UPLSAPO). Excitation at 639 nm was provided by a pulsed diode laser head (LDH-P-C-635-B, PicoQuant GmbH, Berlin, Germany) driven by a picosecond laser driver (LDH-800-B, PicoQuant GmbH, Berlin, Germany). The fluorescence from the sample was collected by the water objective and spatially filtered using a 50 µm pinhole. The fluorescence from the dye was passed through an emission filter (HQ 675/50m, Chroma Technology Corp., VT, USA), and focused onto a single-photon avalanche photodiode (SPCM-AQRH 14, Perkin Elmer Inc., USA). The signal from the diode was read out by using a TimeHarp200 counting board (PicoQuant GmbH, Berlin, Germany). The power used for the calibration and for other FCS measurements amounted to 20 µW, as measured after the objective, corresponding to a specific power of ~4.3 kW/cm^2 at the sample. For both, ATTO655 in pure buffer and ATTO655 in sucrose solution, five FCS experiments were performed. The dye concentrations were 100 pM, 250 pM, 500 pM, 1 nM, 2 nM.

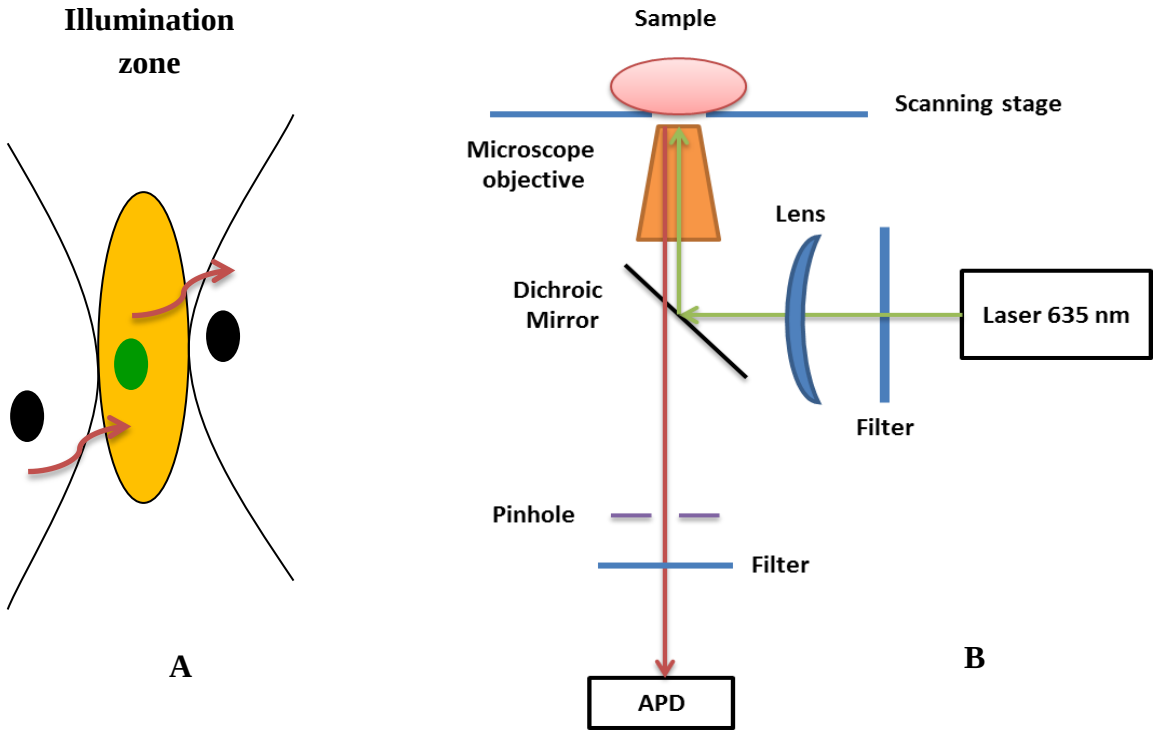

Figure 2.2: *(A) Representation of the effective volume (yellow) where molecules move freely in the solution; the black dot represents a labeled molecule and it turns fluorescent (green) when it is in the effective volume, (B) Scheme of the confocal setup used for the measurements.*

2.2.5 *Fluorescence Lifetime Correlation Spectroscopy (FLCS) data acquistion*

For the acquisition of FLCS data, the sample was deposited on a cleaned glass slide and covered with the cap of a polypropylene test tube to avoid evaporation of the solvent during the measurements. A new cap was used for each measurement to avoid sample cross-contamination. For each experimental condition, time traces were recorded for durations varying from 5 to 10 minutes, depending on the conditions of the experiment. The raw data were stored as time-tagged time-resolved (t3r) data files and subsequently elaborated using the SymPhoTime software package. To eliminate the detector afterpulsing and other sources of noise due to detector imperfections, the single photon arrival time data were filtered as described in reference (*15*). For this, the internal dedicated routine of the SymPhoTime software package was used. Briefly, after acquisition of the data, the time correlation single-photon counting (TCSPC) histogram for the measurement was built. After narrowing down the time window of the TCSPS decay, fitting was performed with an exponential function as described in ref. (*16*). Based on the fitted values the software automatically generated a set of filter functions. The filter functions were subsequently used by the software to select the photons for the calculation of the autocorrelation function. The autocorrelation from the single-photon counting data was calculated using the SymPhoTime software package and the data were analyzed using FCS equation as described in the section 2.3.

2.2.6 *Preparation of glass slides*

Round glass coverslips with 0.25 mm thickness (Marienfeld**,** VWR International) were used for all FCS measurements. They were first cleaned with methanol and then treated with 4.0M sodium hydroxide, each step taking 30 minutes at room temperature. Afterwards, the coverslips were rinsed several times with Milli-Q water and then sonicated in acetone for 15-20 minutes. The coverslips thus prepared were stored in Milli-Q water. A confocal image of a cleaned glass slide is presented in Fig. 2.3. For nano-rod coating, ozone cleaned glass coverslips were prepared using UVO-Cleaner Model 42-220, Jetlight Company Inc., Irvine, California, USA.

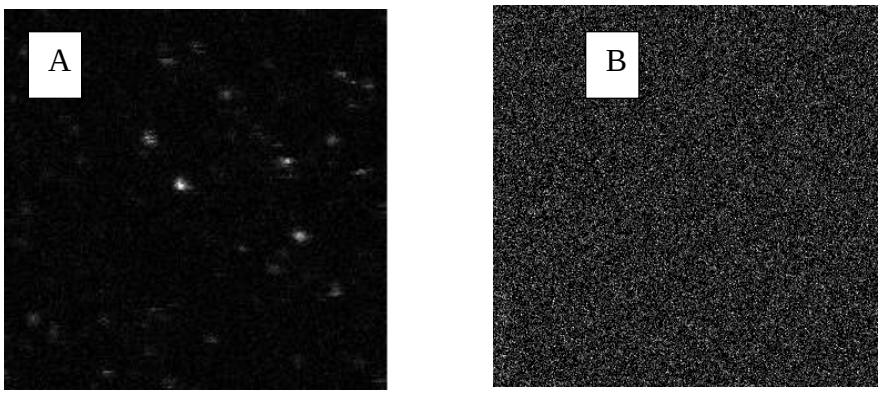

Figure 2.3: *40×40 μm^2 images taken under confocal fluorescence microscope of a glass slide: (A) before and (B) after cleaning.*

2.2.7 *Preparation of gold nano-rods*

The gold nano-rods were first prepared with the seed-mediated growth method as described in the literature(*17*). A surfactant called Cetyl-trimethylammonium bromide (CTAB) was added to a suspension of gold nano-rods in the buffer. The excess amount of CTAB was washed out and the rods were dispersed into Milli-Q water. The nano-rods thus prepared, had average dimensions of 45 nm × 100 nm. Their longitudinal plasmon resonates around 640 nm in water. The nano-rods were spin-coated on a cleaned glass surface using a spin-coater (SpinCoater Model P6700 Series, Specialty Coating System Inc., West Minnesota, Indianapolis, USA) in two spinning steps: 2000 rpm for 30 sec and 4000 rpm for another 30 sec.

2.3 *FCS calibration: results and discussion*

ATTO655 was chosen for labeling purposes since its properties have been thoroughly documented by Sauer, Tinnefeld and others((*18*)(*19*)(*20*)(*21*)(*22*) and references therein). This dye is not easily oxidized whereas the reduced form is quickly oxidized back by oxygen. Under aerobic conditions the dye is stable, shows little blinking and is not easily bleached.

2.3.1 *Calibration of the probe volume*

For the FCS measurements, a typical sample consists of a dilute water-based solution of fluorescently labeled molecules. A laser beam is focused in the sample with a high numerical aperture lens creating a measurement volume with a diffraction-limited spot (Fig. 2.2A). When

using a dichroic mirror, a micrometer size pinhole, lens and beam splitter, only fluorescence originating from the measurement volume is collected. A typical range of pinhole diameters is 30-100 µm. The pinhole is used to reject the out-of-focus light. The emitted fluorescence is projected onto an avalanche photo diode (APD) and the autocorrelation function (ACF) is generated. Analysis of the ACF gives us information about the time scale of the diffusion (τ_D), the diffusion coefficient (D) and the number of molecules <N> in the effective volume. τ_D depends on the size and shape of the measurement volume, referred to as effective volume, V_{eff} of the setup. It is necessary to know beforehand the size and shape of the effective volume. Therefore, calibration of the setup is important and it is about determining the size of V_{eff}.

For calibration of the effective volume in 20 mM HEPES pH 7.0 buffer and in 57% (w/w) sucrose, it is assumed that the light intensity in the effective volume exhibits a three dimensional Gaussian profile i.e. the intensity of the laser beam is represented by the formula:

$$I = I_0 e^{-2(x^2+y^2+\frac{z^2}{k^2})/r^2}$$

where I_0 describes the intensity at the center of the laser beam and x, y and z represent the three coordinates of the illuminated volume (Fig. 2.1). Thus the confocal volume is an ellipsoid where the ellipse is rotated around the long axis.

The autocorrelation function has the form:

$$G(\tau) = G(0) \cdot \left(1+\frac{4D\tau}{r_0^2}\right)^{-1} \cdot \left(1+\frac{4D\tau}{z_0^2}\right)^{-1/2} \quad (2.1)$$

$$= G(0) \cdot \left(1+\frac{\tau}{\tau_D}\right)^{-1} \cdot \left(1+\left(\frac{r_0}{z_0}\right)^2 \frac{\tau}{\tau_D}\right)^{-1/2} \quad (2.2)$$

$$= G(0) \cdot \left(1+\frac{\tau}{\tau_D}\right)^{-1} \cdot \left(1+\frac{\tau}{k^2\tau_D}\right)^{-1/2} \quad (2.3)$$

where $G(\tau)$ is the auto-correlation function, D is the diffusion coefficient of the molecule of interest, τ_D is the residence time of the molecule in the confocal volume and r_0 and z_0 denote the distances from the center of the confocal volume where the intensity has dropped by a factor of $1/e^2$ in the radial and axial direction, respectively. The diameter of the diffraction limited spot

depends on the wavelength λ of the probing light and the lens-numerical aperture for the measurements.

Single molecule FCS measurements possess some intrinsic limitations. One of the pitfalls is refractive index changes in solutions. It can cause distortions of the effective volume. Such distortions appear in particular polymer solvents e.g. sucrose, glycerol-solution. Creating different models with distorted volume is a hard even impossible task. For FCS analysis, we assumed an ellipsoid shape of the effective volume in 57% w/w sucrose solution similar that in buffer and determined V_{eff} in 57% w/w sucrose solution. Apart from the refractive index, slight changes in coverslip thickness, pinhole adjustments, laser beam geometry or optical saturation can lead change in the effective volume.

One way to determine the confocal parameters is by plotting *G(0)* as a function of the concentration of the dye (Eqn. (2.4)). If the measured signal fluctuations are only due to the diffusion, the amplitude of autocorrelation function equals to the inverse number of the fluorescence molecules present in the effective volume V_{eff} on average. Using a dilution series of labeled sample, the effective volume can be determined(*11*),

$$G(0) = \frac{1}{\langle N \rangle} = \frac{1}{c \cdot V_{eff} \cdot N_A} \qquad (2.4)$$

where <*N*> is the average number of particles in the probe volume, *c* is the concentration of the dye, V_{eff} is the effective probe volume, and N_A is Avogadro's constant 6.022×10^{23} mol^{-1}. V_{eff} is approximated with three-dimensional Gaussian shape function and is larger than the confocal volume(*23*) by a factor of $2^{(2/3)}$.

$$V_{conf} = \left(\frac{\pi}{2}\right)^{3/2} r_0^{\,2}\, z_0 = \left(\frac{1}{2}\right)^{3/2} V_{eff} \qquad (2.5)$$

First the autocorrelation amplitudes of a dilution series of ATTO655 in buffer and sucrose were determined experimentally. Two datasets for FCS curves for buffer and 57% (w/w) sucrose solution have been presented in Fig. 2.4 and Fig. 2.5. The concentrations of dye used were: 2.0, 1.0, 0.5, 0.25, and 0.1 nM. A plot of <*N*> values versus the dye concentration was obtained (Fig. 2.6). The slope of a linear fit of the data corresponds to $V_{eff}N_A$ from which the size of the effective volume was calculated (Fig. 2.6). In buffer, V_{eff} was 2.3±0.2 fL and in 57%

(w/w) sucrose solution it was 2.9±0.1 fL. This approach is model free: it makes no assumptions about the geometry of V_{eff} or the diffusion model. It only measures the correlation amplitude of a series of samples with known concentrations.

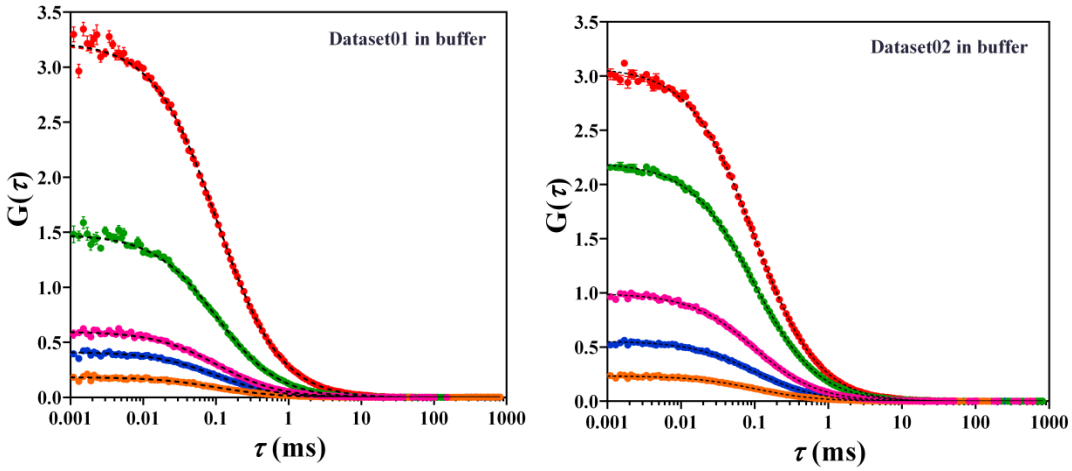

Figure 2.4: *FCS traces of ATTO655 obtained in the buffer. Two datasets are shown here. The buffer used was 20 mM HEPES pH 7.0 and the concentration of the dye was 2.0 (orange), 1.0 (blue), 0.5 (pink), 0.25 (green), and 0.1 (red) nM. The dots are experimental data points and dashed lines are fits of the data. Error bars denote the standard errors as obtained from the fitting procedure.*

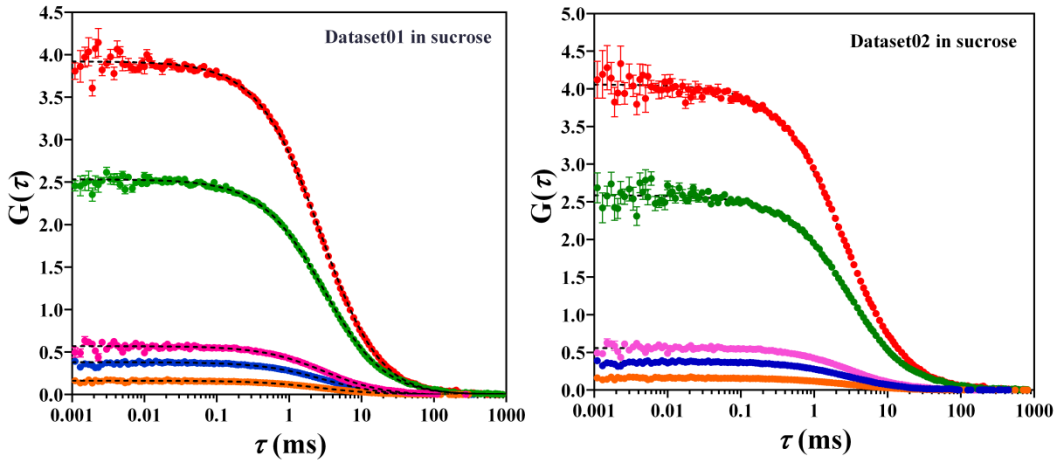

Figure 2.5: *FCS traces of ATTO655 obtained in 57% (w/w) sucrose solution. Two datasets are shown here. The buffer used was 20 mM HEPES pH 7.0. The concentration of the dye was 2.0 (orange), 1.0 (blue), 0.5 (pink), 0.25 (green), and 0.1 (red) nM. The dots are experimental data points and dashed lines are fits of the data. Error bars denote the standard errors as obtained from the fitting procedure.*

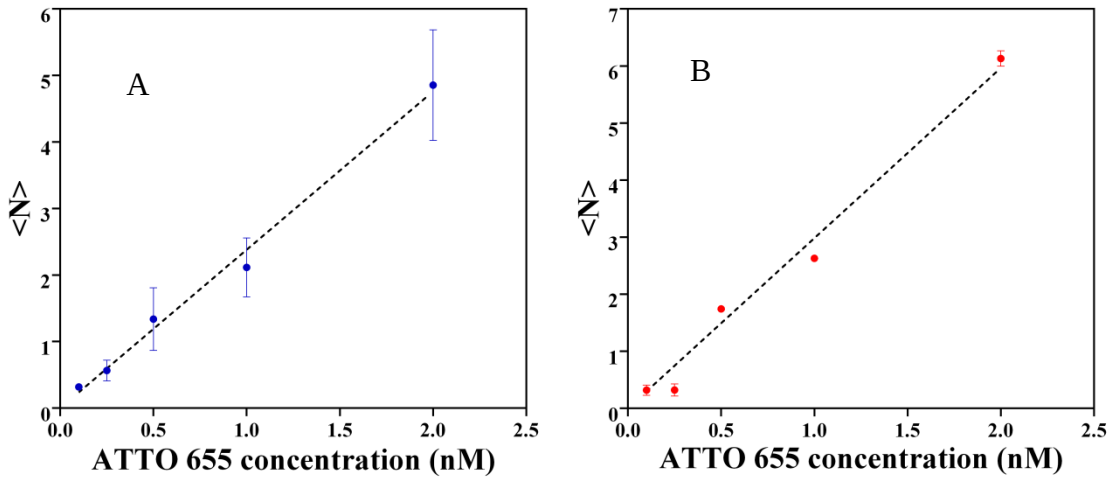

Figure 2.6: *Plots of <N> as a function of the ATTO655 concentrations in: (A) 20 mM HEPES buffer pH 7.0 and (B) 57% (w/w) sucrose solution. In both, the black dashed lines are linear fits of the data. (Average values of <N> from two datasets for buffer and 57% (w/w) sucrose solution (See Figs. 2.4 and 2.5) have been used to plot)*

The other way to determine the probe volume is by fitting the autocorrelation data (Fig. 2.4 and 2.5) with Eqn. 2.3 using a weighted least-square Levenberg-Marquardt method, where the variance of each data point is used as a weighting factor. First, with known diffusion coefficient of ATTO655 in water (426μm^2 s^{-1}), the diffusion coefficient of ATTO655 in 57% w/w sucrose solution was estimated according to the Stokes-Einstein law (see 2.4 section). The diffusion coefficient was found to be 11.0μm^2 s^{-1}. Next, GraphPad Prism 5 and 6 (GraphPad Inc. USA) was used as the fit program for fitting the autocorrelation data. After fitting the autocorrelation curves obtained from a dilution series of ATTO655 in the pure buffer, the resulting parameters were 386±1 nm and 6.5±0.2 for r_0 and k respectively (Fig. 2.7). The effective volume was calculated by $V_{eff} = \sqrt{\pi^3} k r_0^3$ (see Eqn. 2.5) giving V_{eff} = 2.1±0.5 fL. Then, the same procedure was applied to calibrate V_{eff} for the 57% (w/w) sucrose stock solution resulting in r_0 = 389±2 nm, k = 3.8±0.4, and V_{eff} =1.3±0.2 fL, respectively. The experimentally obtained "k" value in 57% (w/w) sucrose solution was used for the fitting of the ACFs of labeled azurin samples (Chapter 3, 4 and 5).

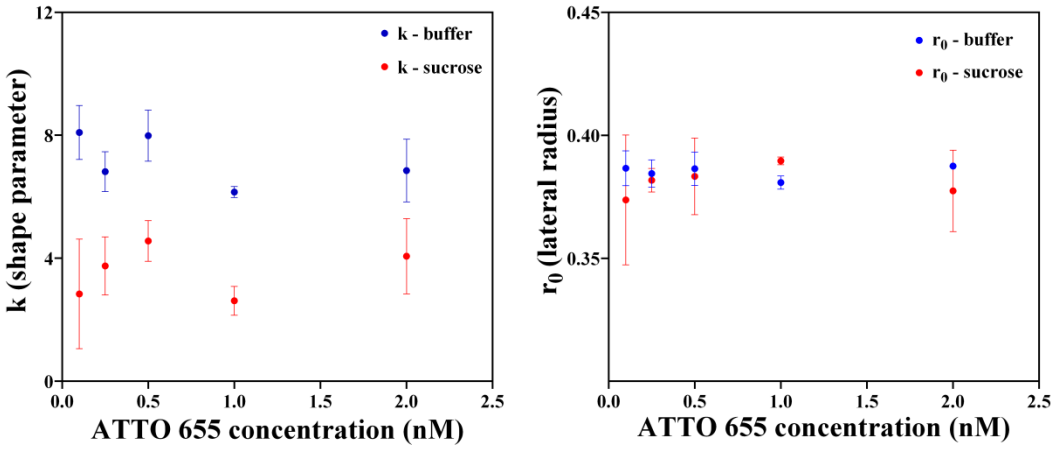

Figure 2.7: *Experimentally obtained parameters (k, r_0) for dilution series of ATTO655 in (A) buffer and (B) 57% (w/w) aqueous sucrose solution.*

From the fits of the ACFs also τ_D was determined (See Fig. 2.4 and 2.5). The average diffusion times for the dye as obtained from the fits amounted to 0.102 ± 0.01 ms (water) and 2.9 ± 0.3 ms (57% w/w sucrose solution) (Fig. 2.8). On the basis of the known diffusion coefficient of ATTO655 in water (D = 383 µm^{2}s^{-1}) and r_0 = 385 nm a value of 0.097 ms is calculated for τ_D (Eqn. 2.7), in good agreement with the experimentally determined value. Diffusion coefficient depends on the viscosity of the solution (see section 2.4, Eqn. 2.11). In the present case, as the viscosity increases by a factor of 40 going from 0% sucrose solution to 57% (w/w) sucrose solution, the increase of the diffusion time is by a factor of 29 (Fig. 2.8).

$$\tau_D = \frac{r_0^{\,2}}{4D} \qquad (2.7)$$

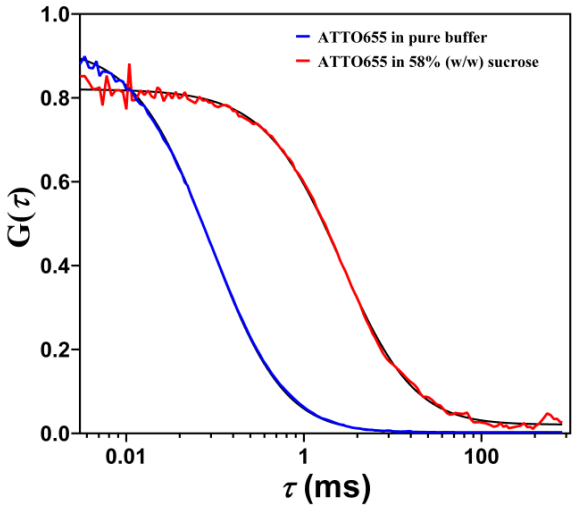

Figure 2.8: *Experimentally obtained ACFs for ATTO655 in buffer (red) and 57% (w/w) sucrose (blue) solution. The black lines are the fits according to the Eqn. $G(\tau) = G(0)G_{diff}(\tau)$, with τ_D = 0.102 ms in pure buffer and τ_D = 2.9 ms for the 57% (w/w) sucrose solution.*

2.3.2 *Determination of confocal volume by nano-rod scanning*

It was an additional interest for us to determine the effective volume based on the imaging of gold nano-rods. Besides laser excitation power, the measurement conditions were kept similar as mentioned for previous FCS calibration measurements (see Section 2.3.1 for details). The nano rods are treated as point sources and can be used in order to scan the volume.

Sample medium	***x*** (r_0) (µm)	***y*** (µm)	***z*** (axial z_0) (µm)	***k***	V_{eff} (fL)
Air	0.424	0.419	1.953	4.6	1.9
Buffer	0.380	0.455	1.579	4.2	1.2
70% (w/v) sucrose	0.520	0.590	1.895	3.6	2.8

Table 2.2: *Experimentally obtained dimensions of the effective volume in micrometers determined from Gaussian fits of the sections shown in Fig. 2.9. Mean values are shown here.*

For effective volume determination, the MicroTime 200 system equipped with an axial piezo positioner was used to scan the nano-rod coated glass substrate. It can scan in the lateral xy-as well as in the axial xz-plane. The scanner accuracy is ±3.0 nm and can be disregarded as a source

of uncertainty. Approximately 200 µl of buffer or sucrose solution was added on the surface of the nano-rod deposited glass slides and then the imaging was performed. First, an overview image was taken from which bright spots were selected for further analysis. Then, from those bright spots, sectional scans were recorded in a plane, e.g. *xy*-scan. Then, they were fitted with a two-dimensional Gaussian distribution as described in the application note of PicoQuant(*11*). In the present work, three scanning measurements were performed under air, water and in 57% (w/w) aqueous sucrose solution respectively. Fig. 2.9 shows the images of 2D sections for the effective volumes in air, buffer and sucrose solution. The experimentally obtained effective volume under different conditions with the lateral radius (r_0) and the eccentricity (k) have been summarized in Table 2.2. Using the lateral and axial dimensions, extracted from the different sections of the volume, V_{eff} is calculated according to Eqn. 2.8 as described in ref.(*11*):

$$V_{eff} = \pi^{(3/2)}. \text{ x. y. z (fL)} \qquad (2.8)$$

Although the imaging method resulted in slightly different values for V_{eff}, the calculated volume was found to be similar to the values (1-2 fL) reported in See section 2.3.1.

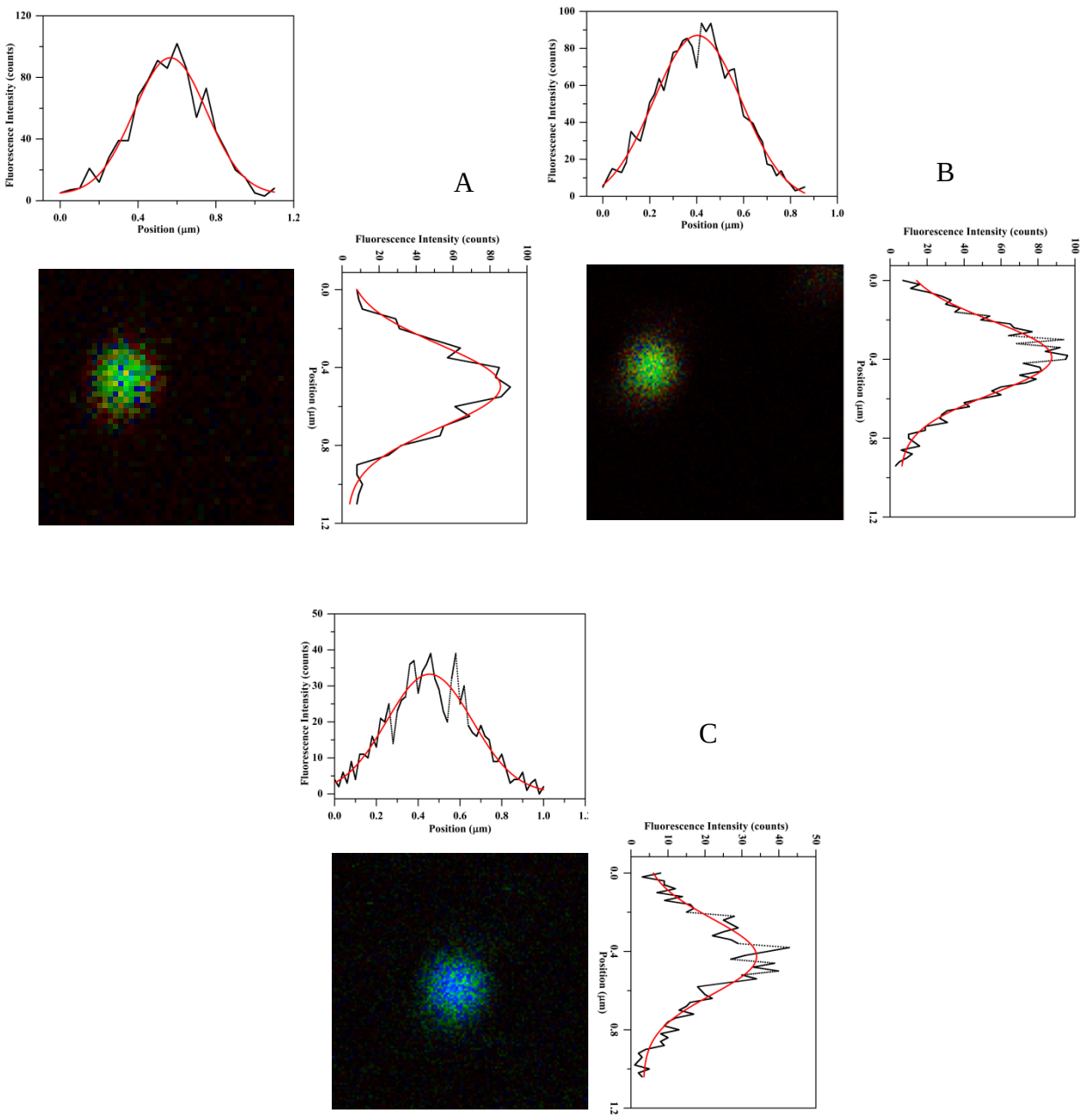

Figure 2.9: *xy sections of the effective volumes, measured with 45 nm × 100 nm gold-nano rods in (A) air (B) buffer and (C) 57% (w/w) sucrose solution (z is along the optical axis). Along with the 2D sections line profiles through the center positions are shown. Experimental data are shown in black whereas line sections of the 2D Gaussian fits are represented by red.*

2.4 *Diffusion, bimolecular interactions and their dependency on viscosity*

In the present thesis, we have investigated short-time-scale dynamics such as photoinduced electron transfer reactions in azurin-dye constructs or the blinking of the dye in the presence of redox agents by fluorescence correlation spectroscopy. We need to consider reactions of the label with a) chemicals in solution (intermolecular reactions) and b) the metal center in the protein (intramolecular reactions). The intermolecular reactions between the label (ATTO 655) and the redox agents (ascorbate, potassium hecacyanoferrate (III)) depend on the diffusion times of those molecules. To assess this, we look into the diffusion time scales of labeled proteins and into the rates of the bimolecular reaction between the labeled azurin and redox agents. What are the association rates and how do they vary as a function of viscosity?

When reactions between molecules occur at every collision, the reaction is diffusion controlled. Association rates in solution are determined by the time it takes to bring reactive partners together by diffusion. Such association reactions, in general, have very small activation barriers and diffusion controlled reactions have rates of $k_d = 10^9$-10^{10} $M^{-1}s^{-1}$ in aqueous solution at room temperature(*24*)(*25*). In the present work, the reaction between the redox chemicals and the dye is diffusion controlled (See Chapter 3 for details). After the redox reaction, the dye enters into a dark state. To be observable by FCS, the reaction between the redox agent and the label has to take place within the time it takes for the labeled protein to cross the effective volume.

As mentioned earlier, the diffusion can be varied by varying the viscosity (η) of the solution. A rough estimate of the diffusion time of azurin in a sucrose solution can be obtained from the rule of thumb that τ_D is proportional to the cube root of the molecular weight(*26*). With a molecular weight 13998 for azurin and 887 for ATTO655 and a diffusion time of 2.9 ms for ATTO 655 in 57% (w/w) sucrose solution (See page 13), the estimated diffusion correlation time for azurin in 57% (w/w) sucrose solution would amount to 7 ms. Single molecule FCS measurements on labeled zinc azurin samples in pure buffer showed that the diffusion time amounted to 200 µsec, which shifted to the millisecond range when a 57% (w/w) sucrose solution was used. The average diffusion time was found to be 12±2 ms (Fig. 2.10) in agreement with expectation.

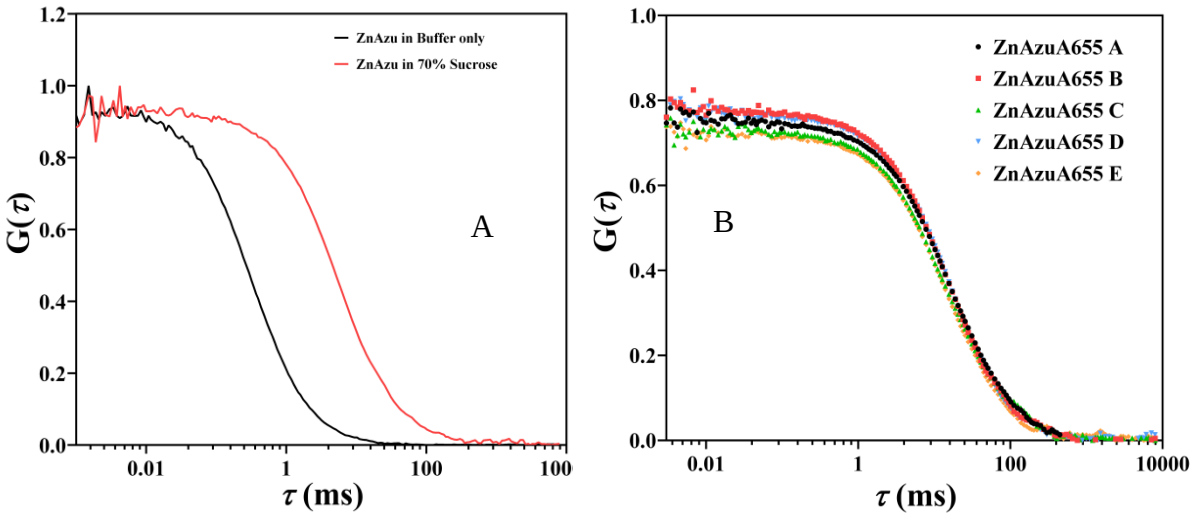

Figure 2.10: *(A) Experimentally obtained ACFs for ATTO655 labeled Zn azurin in buffer and 57% (w/w) aqueous sucrose solution without redox agents. (B) ACFs of ATTO655 labeled ZnAzu prepared in 57% (w/w) sucrose solution without redox chemicals for five sets of experiments.*

Within the sucrose concentration range from 70 %(w/v) to 60 %(w/v), the diffusion correlation time of labeled azurin changes from 12 to 3 ms. This range is preferred for FCS measurements if we want to study any microsecond dynamics (blinking, electron transfer, conformational changes etc.) in the sample. Our next interest was to estimate the bimolecular rate constants between the label and the redox agents. How is it assessed?

The diffusion controlled bimolecular reaction rate k_d can be estimated from Smoluchowski's principle(*27*)(*28*)(*29*)

$$k_d = 4\pi(D_A+D_B)(r_A+r_B) = 4\pi D_{AB}R_{AB} \qquad (2.9)$$

where D_A and D_B are the diffusion constants (in cm^2s^{-1}) and r_A and r_B are the hydrodynamic radii (in cm) of the reacting spherical molecules, respectively. The unit of k_d is $M^{-1}\ s^{-1}$. $R_{AB} = (r_A + r_B)$ is the minimal distance between the centers of the two molecules. The diffusion constant for their relative motion is represented by $D_{AB} = D_A + D_B$. In the present case, we are dealing with molecules of different size (e.g. hexacyanoferrate (III), ATTO655, azurin). The diffusion of redox agents, e.g., sodium ascorbate is rapid in the solution compared to that of large azurin protein (~ 3 nm). The labeled azurin and the redox chemicals are assumed to be spherical in shape with $r_A >> r_B$. If D_{AB} is in the order of 10^{-7} cm^2s^{-1} for small proteins(*30*)(*31*) and R_{AB} is close

to 1 Å, the bimolecular rate constant amounts to ~7×10^{8} $M^{-1}s^{-1}$ at ambient temperature using Eqn. 2.9. For small molecules with D in the order of 10^{-5} $cm^{2}s^{-1}$, this rate constant can reach ~10^{10} $M^{-1}s^{-1}$ in aqueous solution(*32*)(*33*)(*34*). This is the maximum diffusion controlled bimolecular rate, known as Smoluchowski's limit.

Another aspect is that ATTO655 labeled azurin is not reactive over its entire surface. For a labeled species, the dye is attached to a particular position on the protein surface. The oxidant or reductant will have productive associations with only a fraction of the total surface area of azurin. The reaction rate will depend on the fraction of the reactive configurations of labeled molecules in solution. For this, we consider the molecules to be spherical: molecule A (labeled protein) and molecule B (redox agent). The labeled protein A of radius r_A is chosen at the origin of a spherical polar coordinate system (r, θ). B molecules are uniformly reactive over their entire surfaces. The surface of the labeled protein is reactive only over the axially symmetric range $0<\theta<\theta_0$. A reactive encounter may only occur if the redox agent is located within the reaction radius R_{AB} and within the range $0<\theta<\theta_0$ over the protein surface (Fig. 2.10). It has been calculated(*35*) that

$$k_d = 4\pi D_{AB} R_{AB} \sin(\theta_0/2) \qquad (2.10)$$

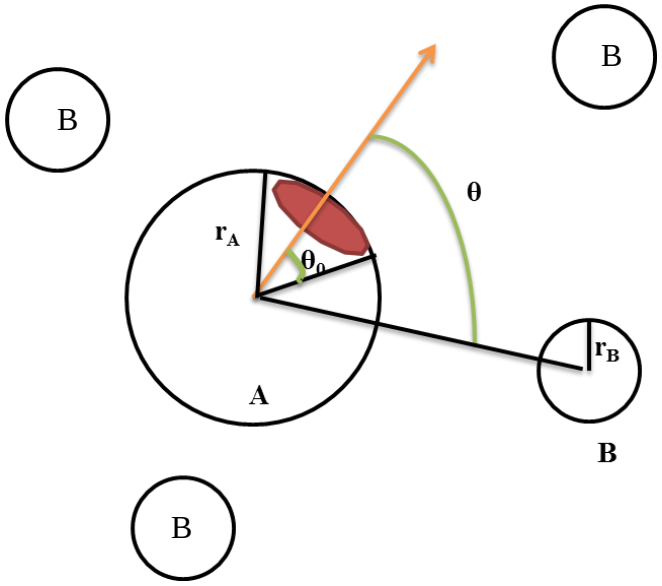

Figure 2.11: *Schematic diagram of the reactive-patch geometry of the association complex [molecule A with reactive surface patch (red)]. As discussed in the text, an association is assumed to take place only after the two molecules have come into contact. The red area shows the reactive patch for the labeled protein. The redox agents (B) are spherical and assumed to have homogeneous reactivity over their entire surface. (Adapted from Biophysical Journal, 1981, volume 36, pp. 697-714)*

If there are severe steric constraints, θ_0 may become very small, which will reduce the maximum diffusion controlled bimolecular rate considerably. There are many other factors which can affect the association rate constants e.g. short range forces, the presence of receptors on the molecular surface, coupling of the diffusion processes(*27*)(*28*)(*29*)(*36*).

As mentioned previously (see section 2.3), according to the Stokes-Einstein law, the diffusion coefficient depends on the viscosity of the solution as well as the temperature:

$$D = k_B T/6\pi\eta r \qquad (2.11)$$

It predicts that the application of a high viscosity liquid such as a sucrose solution or glycerol can slow down the diffusion processes as $k_d \propto 1/\eta$. In glycerol (viscosity 950 cP), k_d may reach values of 10^6 M^{-1} s^{-1}. As a consequence, the reactions between the label and redox agent will be slowed down. A flurry of experiments have been performed to understand the variation of association rates as a function of diffusion coefficients and

viscosities(*29*)(*37*)(*36*)(*38*)(*39*)(*40*)(*41*)(*42*)(*43*)(*44*). In our work, the use of 57% (w/w) sucrose has increased the viscosity by a factor of 40 (Table 1), which suggests that k_d can reach 10^7-10^8 $M^{-1}s^{-1}$ in 57% (w/w) sucrose solution compared to 10^9-10^{10} $M^{-1}s^{-1}$ in buffer. Using labeled ZnAzu, the rates of reaction between the redox agents and the labeled protein have been experimentally obtained from single molecule FCS measurements and will be discussed in Chapter 3.

2.5 *Photobleaching and blinking of fluorophore*

The use of organic fluorophores and fluorescent proteins in biochemical and biophysical applications of single-molecule spectroscopy is a common practice now-a-days(*45*)(*46*)(*47*)(*48*)(*49*). It is important to choose the appropriate fluorescent probe in order to be able to interpret the results for each experiment. For this it becomes essential to understand the photochemical and photophysical processes of the dyes. We briefly discuss the photophysical processes in this section. Photoinduced processes of a dye can be observed in various ways (Fig. 2.12). After photoexcitation, either the excited molecules return directly to the ground state via fluorescence (radiative process) or non-radiative decay or the molecules decay to triplet states via intersystem crossing. Since the rate of conversion of a triplet state to the ground state is slow due to spin conversion, the molecules stay in the triplet state for a long time. In solution, when such deactivation processes are not too fast, i.e., when the lifetime is sufficiently long, a molecule in the triplet state has a chance to react with other molecules in the surrounding medium. For example, dissolved oxygen, which has a triplet ground state, can react with fluorophores in the triplet state, leading to free radicals that are toxic to cells. On the other hand, during photobleaching, a fluorophore permanently loses the ability to fluoresce due to photon-induced chemical damage or covalent modification. Fluorophores in the excited singlet or triplet state also can react with other small molecules or biomolecules. For fluorophores in solution, redox blinking can be easily induced by the presence of oxidants such as oxygen, methylviologen or by reductants such as ascorbate, DTT, potassium hexacyanoferrate (II) etc. For example, Vogelsang *et al.* in 2008 showed that the blinking process can be altered by changing the ratio of reducing agents and oxygen in the solution(*50*). Molecules containing heavy atoms, such as the halogens and transition metals, often facilitate intersystem crossing resulting in blinking. Therefore, photobleaching and blinking of fluorescent dyes must be controlled carefully, especially for single molecule analysis. Single-molecule measurements have

been carried out to understand the blinking properties of the conventional dyes(*50*)(*51*)(*52*)(*53*)(*54*)(*55*). Mainly, the excitation conditions and local environment have been varied to determine the various causes for the blinking.

Studies also have been performed to understand photoinduced electron-transfer reactions involving fluorescent labels attached to the proteins(*22*)(*50*)(*53*)(*56*)(*57*)(*58*)(*59*)(*60*)(*61*)(*62*)(*63*). To a lesser extent, the propensity of the label to engage in redox reactions with protein residues and protein cofactors has been studied for some fluorescent labels. In case of proteins, tryptophan was not the only moiety to show redox activity towards the fluorescent probes, metal cofactors, NADH, FAD, porphyrins and tyrosines also can show such activities.

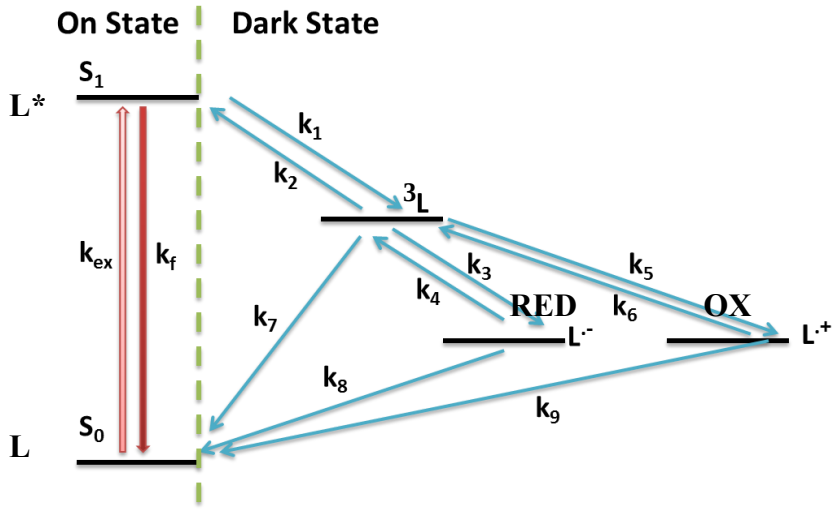

Figure 2.12: *A "Jablonski diagram" of a fluorophore. The fluorophore (L) is excited from its ground state (S_0) to the first excited state (S_1) with an excitation rate k_{ex} and it fluoresces with the rate k_f with a lifetime of a few nanoseconds. Competing processes are non-radiative decay to S_0 and intersystem crossing to the triplet state (^3L) (k_1, k_2). If an oxidant or a reductant is added, the triplet state may be depopulated quickly and radical cations ($L^{\cdot+}$) or anions ($L^{\cdot-}$) (k_3, k_4, k_5, k_6) are formed, respectively. The triplet state can also return to S_0 (k_7) by a radiative process (phosphorescence). Depending on the redox potentials, these dark states ($L^{\cdot+}$, $L^{\cdot-}$) are comparatively stable but can be returned to S_0 by the complementary process in a buffer containing a reducing as well as an oxidizing compound (k_8, k_9).*

In the present thesis, blinking of the fluorophore and photoinduced electron transfer in a labeled azurin have been investigated in detail. It is shown how single molecule FCS can be utilized to analyze diffusion, blinking and PET in a labeled sample.

2.6 *Photoinduced electron transfer (PET)*

We have discussed in chapter 1 the electron transfer between a donor and an acceptor. This reaction can be thermally or photochemically induced. In recent years, photoinduced electron transfer reactions (PET) have been a studied (*64*)(*65*)(*66*)(*67*)(*68*)(*69*). Photoinduced intramolecular and intermolecular electron-transfer reactions are of special interest due to their importance in photosynthesis, photochemical reactions, photoimaging, solar energy conversion and many other applications(*70*)(*71*)(*72*)(*73*)(*74*). For bimolecular electron transfer between two species in their ground states, the standard free energy change is given by

$$\Delta G^{0}_{CS} = IP_D - EA_A \qquad (2.12)$$

where, IP_D is the ionization potential of the donor and EA_A is the electron affinity of the acceptor. These quantities are estimated from the energies of the highest occupied molecular orbital (HOMO) and lowest unoccupied molecular orbital (LUMO) orbitals of the donor and the acceptor, respectively. The PET reaction takes place when a short pulse of light activates an electron-rich molecule, and an electron is transferred from the HOMO to the LUMO of the donor and from there to the LUMO orbital of the electron deficient acceptor. When the donor absorbs light and gets excited, it changes the redox properties of the donor.

$$D \xrightarrow{h\nu} D^{*}$$

Then, it interacts with the acceptor, and there is formation of a short-lived intermediate called the encounter complex. If we consider the PET reactions in solution, the lifetimes of these complexes are of the order of nanoseconds, and the quenching occurs by the acceptor i.e. it accepts the electron from the donor.

$$D^{*} + A \longrightarrow D^{+\bullet} + A^{-\bullet}$$

Now, (IP_D - EA_A) decides the feasibility of electron transfer between donor and acceptor in the ground state. According to Rehm and Weller(*75*), for photoinduced electron transfer between an a donor (*D*) and the acceptor (*A*) (either one of them may be the electronically excited molecular entity), the change in standard Gibbs free energy can be approximated as

$$\Delta G = eE_{D^+/D} - eE_{A/A^-} - \Delta G_{0,0} + (n_A - n_D - 1)\frac{e^2}{\varepsilon d} \qquad (2.13)$$

which describes the driving force ΔG for the ET by a donor (D) to an acceptor (A) with $E_{D^+/D}$ and E_{A/A^-} denoting the midpoint potentials of donor and acceptor, respectively. Here, either the donor or the acceptor is optically excited with $\Delta G_{0,0}$ denoting the energy of the corresponding optical *0-0* transition, e denotes the electronic charge, d the distance between donor and acceptor, ε the dielectric constant and n_A and n_D the charges of acceptor and donor in units of $|e|$, respectively. Eqn. 2.13 has been used to calculate the driving forces of the PET reactions in Cu azurin-ATTO655 bioconjugate (See chapter 4). In addition to PET, various other processes may occur e.g. formation of chemical products, radiative and non-radiative decay, intersystem crossing.

A number of studies have been reported to determine the distance and medium dependence of the electronic coupling in proteins ((*76*)(*77*)(*78*)(*79*)(*80*) and references therein). Motivated mostly by the reaction mechanism of respiratory electron-transport chains and electron-transfer reactions in redox enzymes, various experiments have been performed for a precise understanding of PET rates in relation to reorganization energies of the proteins, dependence on redox potentials of donor and acceptor etc. For reviews of these achievements the reader is referred to the literature (*81*)(*82*)(*83*)(*84*)(*85*). Gray and coworkers, made major contributions in understanding PET reactions in metalloproteins like azurin. They explored the distance dependence of ET tunneling through the folded organic framework of the protein by employing surface-attached coordination compounds(*83*).

Ruthenium and osmium compounds were attached at several locations in the β-strand structure of azurin and the driving-force dependence of ET between reduced Cu(I) and oxidized Ru(III) or Os(III) was examined by laser-flash quench studies. The distance between the redox centers was varied from 16 to 26 Å depending on the position of the label on the strand. The ET times were found to increase exponentially from microseconds to milliseconds with increase in the distance between the donor and acceptor. Close van der Waals contact (3 Å) between two redox centers results in a 10^{13} s^{-1} ET rate. The results basically show that beyond this distance (26 Å) multiple tunneling steps are required for efficient ET reaction. Analysis of labeled azurin

with Ru(III) or Os(III) metal complexes provided the driving forces and reorganization energies for ET reaction between the two redox centers allowing for the calculation of the electronic coupling matrix element and the decay constant (β). In all cases, the reorganization energies and the decay constants were found to be 0.7±0.1 eV and 1.0±0.3 $Å^{-1}$ respectively. Similar ET rates in solution and crystal forms of Ru(III) or Os(III)-complexes suggested that bulk water played a minor role in ET reaction and the intervening protein backbone is necessary for electron-transfer. Gray also found that if Cu(I) is replaced by Zn(II) in Ru-azurin complex, the photogenerated holes remained localized on the Ru center. The ET rates from Cu(I) to Ru(III) did not decrease upon lowering the temperature(*86*)(*87*)(*88*). All these data proved that there was no hopping mechanism operational in photogenerated Ru-azurin complexes.

Onuchic proposed a pathway model which supported Gray's work on ET reaction. The pathway model elaborates the issue of disparate contributions to ET from different pathways connecting the redox centers. Later, it was modified to take into account the anisotropic covalency of the copper site. Other supporting experimental data were provided by Farver and co-workers ((*89*) and references therein). They developed their own scheme for studying long range ET reactions. Their techniques did not require any modifications in azurin. Farver and coworkers investigated the long-range intramolecular electron transfer reactions in azurin by using pulse radiolytically generated CO_2^- radicals to observe the ET reaction between the Cys3-Cys26 bridge (SS^-) in azurin and the oxidized copper ion similar to Ru-complexes(*89*)(*90*)(*91*)(*92*). Similar experiments were performed to understand ET pathways in TUPS-modified (thiouredopyrene-3,6,8-trisulfonate) proteins, where TUPS moieties are attached to surface lysine and cysteine residues(*93*)(*94*)(*95*)(*96*)(*97*)(*98*). Later on, the influence of Trp48 on the ET kinetics was probed by working on azurin variants, where the tryptophan residue was substituted by Ala, Phe, Ser, Tyr, Leu and Met amino acids. Farver and coworkers demonstrated the occurrence of ET by a radical/hopping mechanism through aromatic residues, as demonstrated in Rhenium-azurin complexes. Gray and coworkers also examined multistep tunneling in Re-azurin where Trp is located between Re and the copper center. Cu(I) oxidation was inhibited by the replacement of Trp by Tyr or Phe(*99*)(*100*)(*101*). The effects of solvent dynamics along the ET pathways are also under investigation(*102*). They also have constructed Ru-complexes-azurin systems in which proton-coupled electron hopping mechanism has been demonstrated(*103*)(*104*).

A recent development has been the application of electrochemistry to the study of biological ET reactions. Ulstrup and coworkers have investigated electrode-mediated ET(*105*)(*106*)(*107*)(*108*). Electron microscopic and XPS (X-ray photoelectron spectroscopy) studies of monolayers of azurin adsorbed on gold revealed that azurin is linked via sulphur linkages from the Cys3-Cys26 disulphide bridge to the gold. The measured ET rate of 30 sec^{-1} agreed with the Farver/Petch measurements (44 s^{-1}) compatible with ET from the disulphide interface to the copper center. The low reorganization energy (λ) demonstrated that azurin can retain its activity even with disrupted disulphide bonds and when packed into monolayers on an electrode surface.

The crucial role of the protein framework in determining the electronic coupling still remains a subject of debate. Various calculations have shown that the helix and beta sheet content of a protein and its tertiary structure can influence the distance dependence of ET coupling(*109*). All investigations suggest that the rate of ET in proteins rapidly decreases with distance. Electrons can travel up to 15 Å between the redox centers through the protein medium and an electron can travel much longer distances along a chain of co-factors.

References

(1) Einstein A. von. Über die von der molekularkinetischen Theorie der Wärme geforderte Bewegung von in ruhenden Flüssigkeiten suspendierten Teilchen. *Ann. Phys.* **1905**, *322*, 549–560.

(2) Edward, J. T. Molecular volumes and the Stokes-Einstein equation. *J. Chem. Educ.* **1970**, *47*, 261.

(3) Mason, T. G. Estimating the viscoelastic moduli of complex fluids using the generalized Stokes-Einstein equation. *Rheol. Acta* **2000**, *39*, 371–378.

(4) Magde, D.; Elson, E.; Webb, W. W. Thermodynamic fluctuations in a reacting system measurement by fluorescence correlation spectroscopy. *Phys. Rev. Lett.* **1972**, *29*, 705–708.

(5) Digman, M. A.; Gratton, E. Fluorescence correlation spectroscopy and fluorescence cross-correlation spectroscopy. *Wiley Interdiscip. Rev. Syst. Biol. Med.* **2009**, *1*, 273–282.

(6) Michalet, X.; Weiss, S.; Jäger, M. Single-molecule fluorescence studies of protein folding and conformational dynamics. *Chem. Rev.* **2006**, *106*, 1785–1813.

(7) Chiantia, S.; Ries, J.; Schwille, P. Fluorescence correlation spectroscopy in membrane

structure elucidation. *Biochim. Biophys. Acta* **2009**, *1788*, 225–233.

(8) Widengren, J.; Mets, U.; Rigler, R. Fluorescence correlation spectroscopy of triplet states in solution: a theoretical and experimental study. *J. Phys. Chem.* **1995**, *99*, 13368–13379.

(9) Ha, T. Single-molecule fluorescence resonance energy transfer. *Methods* **2001**, *25*, 78–86.

(10) Majer, G.; Melchior, J. P. Characterization of the fluorescence correlation spectroscopy (FCS) standard Rhodamine 6G and calibration of its diffusion coefficient in aqueous solutions. *J. Chem. Phys.* **2014**, *140*, 6–12.

(11) Rüttinger, S.; Buschmann, V.; Krämer, B.; Erdmann, R.; MacDonald, R.; Koberling, F. Comparison and accuracy of methods to determine the confocal volume for quantitative fluorescence correlation spectroscopy. *J. Microsc.* **2008**, *232*, 343–352.

(12) Hess, S. T.; Webb, W. W. Focal volume optics and experimental artifacts in confocal fluorescence correlation spectroscopy. *Biophys. J.* **2002**, *83*, 2300–17.

(13) Gilani, A. G.; Moghadam, M.; Hosseini, S. E.; Zakerhamidi, M. S. A comparative study on the aggregate formation of two oxazine dyes in aqueous and aqueous urea solutions. *Spectrochim. Acta, Part A* **2011**, *83*, 100–105.

(14) Robert C. Weast, M. J. A. *CRC Handbook of Chemistry and Physics*; CRC Press, Inc, Boca Raton, Florida.

(15) Kapusta, P.; Wahl, M.; Benda, A.; Hof, M.; Enderlein, J. Fluorescence lifetime correlation spectroscopy. *J. Fluoresc.* **2007**, *17*, 43–8.

(16) Kapusta, P.; Macháň, R.; Benda, A.; Hof, M. Fluorescence lifetime correlation spectroscopy (FLCS): Concepts, applications and outlook. *Int. J. Mol. Sci.* **2012**, *13*, 12890–12910.

(17) Nikoobakht, B.; El-Sayed, M. a. Preparation and growth mechanism of gold nanorods (NRs) using seed-mediated growth method. *Chem. Mater.* **2003**, *15*, 1957–1962.

(18) Vogelsang, J.; Cordes, T.; Forthmann, C.; Steinhauer, C.; Tinnefeld, P. Controlling the fluorescence of ordinary oxazine dyes for single-molecule switching and superresolution microscopy. *Proc. Natl. Acad. Sci. U. S. A.* **2009**, *106*, 8107–8112.

(19) Ha, T.; Tinnefeld, P. Photophysics of Fluorescent Probes for Single-Molecule Biophysics and Super-Resolution Imaging. *Annu. Rev. Phys. Chem.* **2012**, *63*, 595–617.

(20) Doose, S.; Neuweiler, H.; Sauer, M. Fluorescence quenching by photoinduced electron transfer: a reporter for conformational dynamics of macromolecules. *Chemphyschem A Eur. J. Chem. Phys. Phys. Chem.* **2009**, *10*, 1389–1398.

(21) Doose, S.; Neuweiler, H.; Sauer, M. Fluorescence quenching by photoinduced electron transfer: A reporter for conformational dynamics of macromolecules. *ChemPhysChem* **2009**, *10*, 1389–1398.

(22) Rasnik, I.; McKinney, S. A.; Ha, T. Nonblinking and long-lasting single-molecule fluorescence imaging. *Nat. Methods* **2006**, *3*, 891–893.

(23) Rüttinger, S.; Buschmann, V.; Krämer, B.; Erdmann, R.; Macdonald, R.; Koberling, F.

Comparison and accuracy of methods to determine the confocal volume for quantitative fluorescence correlation spectroscopy. *J. Microsc.* **2008**, *232*, 343–352.

(24) Wilemski, G. General theory of diffusion-controlled reactions. *J. Chem. Phys.* **1973**, *58*, 4009–4019.

(25) Alberty, R.; Hammes, G. G. Application of the theory of diffusion-controlled reactions to enzyme kinetics. *J. Phys. Chem.* **1958**, *62*, 154–159.

(26) A. Polson, D. V. D. R. Relationship between the diffusion constant and molecular weight. *Biochim. Biophys. Acta* **1950**, *5*, 358–360.

(27) Berg, O. G.; Vonhippel, P. H. Diffusion-controlled Macromolecular Interactions. *Annu. Rev. Biophys. Biophys. Chem.* **1985**, *14*, 131–160.

(28) Strickland, S.; Palmer, G.; Massey, Vi. Determination of Dissociation Constants and Specific Constants of Enzyme-Substrate (or Protein-Ligand) Interactions from Rapid Reaction Kinetic Data. *J. Biol. Chem.* **1975**, *250*, 4048–4052.

(29) Shoup, D.; Lipari, G.; Szabo, A. Diffusion-controlled bimolecular reaction rates. The effect of rotational diffusion and orientation constraints. *Biophys. J.* **1981**, *36*, 697–714.

(30) Young, M. E.; Carroad, P. A.; Bell, R. L. Estimation of diffusion coefficients of proteins. *Biotechnol. Bioeng.* **1980**, *22*, 947–955.

(31) Tyn, M. T.; Gusek, T. W. Prediction of diffusion coefficients of proteins. *Biotechnol. Bioeng.* **1990**, *35*, 327–338.

(32) Collins, F. C.; Kimball, G. E. Diffusion-controlled reaction rates. *J. Colloid Sci.* **1949**, *4*, 425–437.

(33) Hazel, J. R.; Sidell, B. D. A method for the determination of diffusion coefficients for small molecules in aqueous solution. *Anal. Biochem.* **1987**, *166*, 335–41.

(34) Karlsson, O. .; Stubbs, J. .; Karlsson, L. .; Sundberg, D. . Estimating diffusion coefficients for small molecules in polymers and polymer solutions. *Polymer (Guildf).* **2001**, *42*, 4915–4923.

(35) Berg, O. G. Orientation constraints in diffusion-limited macromolecular association. The role of surface diffusion as a rate-enhancing mechanism. *Biophys. J.* **1985**, *47*, 1–14.

(36) Diffusion, R.; Particles, F. Rates of Diffusion-Controlled Relative Diffusion of two Free Particles. *Reactions* 113–118.

(37) Hasinoff BB, Dreher R, D. J. The association reaction of yeast alcohol dehydrogenase with coenzyme is partly diffusion-controlled in solvents of increased viscosity. *Biochim. Biophys. Acta* **1987**, *911*, 53–58.

(38) Andres F. Olea, J. K. T. Rate constants for reactions in viscous media: correlation between the viscosity of the solvent and the rate constant of the diffusion-controlled reactions. *J. Am. Chem. Soc.* **1988**, *110*, 4494–4502.

(39) Feng, C.; Kedia, R. V.; Hazzard, J. T.; Hurley, J. K.; Tollin, G.; Enemark, J. H. Effect of Solution Viscosity on Intramolecular Electron Transfer in Sulfite Oxidase. *Biochemistry*

2002, *41*, 5816–5821.

(40) Kang, S. a; Crane, B. R. Effects of interface mutations on association modes and electron-transfer rates between proteins. *Proc. Natl. Acad. Sci. U. S. A.* **2005**, *102*, 15465–70.

(41) Wenbing Li, Weihong Fan, Bradley O. Elmore, and C. F. Effect of solution viscosity on intraprotein electron transfer between the FMN and heme domains in inducible nitric oxide synthase. **2012**, *585*, 2622–2626.

(42) Ivković-Jensen MM, K. N. Effects of viscosity and temperature on the kinetics of the electron-transfer reaction between the triplet state of zinc cytochrome c and cupriplastocyanin. *Biochemkstry* **1997**, *36*, 8135–8144.

(43) X. Zhang, Johna Leddy, and A. J. B. Dependence of rate constants of heterogeneous electron transfer reactions on viscosity. *J. Am. Chem. Soc.* **1985**, *107*, 3719–3721.

(44) Renat R. Nazmutdinova, Galina A. Tsirlinab, Ibragim R. Manyurova, Michael D. Bronshteina, Nina V. Titovab, Z. V. K. Misleading aspects of the viscosity effect on the heterogeneous electron transfer reactions. *J. Chem. Phys.* **2006**, *326*, 123–137.

(45) Zheng, Q.; Juette, M. F.; Jockusch, S.; Wasserman, M. R.; Zhou, Z.; Altman, R. B.; Blanchard, S. C. Ultra-stable organic fluorophores for single-molecule research. *Chem. Soc. Rev.* **2014**, *43*, 1044–56.

(46) Vogelsang, J. Advancing Single-Molecule Fluorescence Spectroscopy and Super-Resolution Microscopy with Organic Fluorophores. *Physics (College. Park. Md).* **2009**, 1–91.

(47) Yuste, R. Fluorescence microscopy today. *Nat. Methods* **2005**, *2*, 902–904.

(48) Ha, T.; Tinnefeld, P. Photophysics of Fluorescence Probes for Single Molecule Biophysics and Super-Resolution Imaging. *Annu Rev Phys Chem* **2012**, *63*, 595–617.

(49) Willets, K. a.; Ostroverkhova, O.; He, M.; Twieg, R. J.; Moerner, W. E. Novel fluorophores for single-molecule imaging. *J. Am. Chem. Soc.* **2003**, *125*, 1174–1175.

(50) Vogelsang, J.; Kasper, R.; Steinhauer, C.; Person, B.; Heilemann, M.; Sauer, M.; Tinnefeld, P. A reducing and oxidizing system minimizes photobleaching and blinking of fluorescent dyes. *Angew. Chemie Int. Ed.* **2008**, *47*, 5465–5469.

(51) Zondervan, R.; Kulzer, F.; Orlinskii, S. B.; Orrit, M. Photoblinking of rhodamine 6G in poly(vinyl alcohol): Radical dark state formed through the triplet. *J. Phys. Chem. A* **2003**, *107*, 6770–6776.

(52) Christ, Thomas, Florian Kulzer, P. B. Watching the photo-oxidation of a single aromatic. *Angew Chem Int Ed Engl.* **2001**, *40*, 4192–4195.

(53) Heilemann, M.; Margeat, E.; Kasper, R.; Sauer, M.; Tinnefeld, P. Carbocyanine dyes as efficient reversible single-molecule optical switch. *J. Am. Chem. Soc.* **2005**, *127*, 3801–3806.

(54) Vosch, T.; Cotlet, M.; Hofkens, J.; Van Der Biest, K.; Lor, M.; Weston, K.; Tinnefeld, P.; Sauer, M.; Latterini, L.; Müllen, K.; De Schryver, F. C. Probing Förster Type Energy Pathways in a First Generation Rigid Dendrimer Bearing Two Perylene Imide

Chromophores. *J. Phys. Chem. A* **2003**, *107*, 6920–6931.

(55) Orrit, M. Chemical and physical aspects of charge transfer in the fluorescence intermittency of single molecules and quantum dots. *Photochem. Photobiol. Sci.* **2010**, *9*, 637–642.

(56) Dittrich, P.; Schwille, P. Photobleaching and stabilization of fluorophores used for single-molecule analysis with one- and two-photon excitation. *Appl. Phys. BLasers Opt.* **2001**, *73*, 829–837.

(57) Widengren, J.; Chmyrov, A.; Eggeling, C.; Löfdahl, P.-A.; Seidel, C. A. M. Strategies to improve photostabilities in ultrasensitive fluorescence spectroscopy. *J. Phys. Chem. A* **2007**, *111*, 429–440.

(58) Hinkeldey, B.; Schmitt, A.; Jung, G. Comparative photostability studies of BODIPY and fluorescein dyes by using fluorescence correlation spectroscopy. *Chemphyschem A Eur. J. Chem. Phys. Phys. Chem.* **2008**, *9*, 2019–2027.

(59) Stennett, E. M. S.; Ciuba, M. a; Levitus, M. Photophysical processes in single molecule organic fluorescent probes. *Chem. Soc. Rev.* **2014**, *43*, 1057–75.

(60) Cordes, T.; Vogelsang, J.; Tinnefeld, P. On the mechanism of Trolox as antiblinking and antibleaching reagent. *J. Am. Chem. Soc.* **2009**, *131*, 5018–5019.

(61) Cordes, T.; Maiser, A.; Steinhauer, C.; Schermelleh, L.; Tinnefeld, P. Mechanisms and advancement of antifading agents for fluorescence microscopy and single-molecule spectroscopy. *Phys. Chem. Chem. Phys.* **2011**, *13*, 6699–709.

(62) Di Fiori, N.; Meller, A. The Effect of dye-dye interactions on the spatial resolution of single-molecule FRET measurements in nucleic acids. *Biophys. J.* **2010**, *98*, 2265–72.

(63) Chung, H. S.; Louis, J. M.; Eaton, W. Distinguishing between protein dynamics and dye photophysics in single-molecule FRET experiments. *Biophys. J.* **2010**, *98*, 696–706.

(64) Lindstrom, C. D.; Zhu, X. Y. Photoinduced electron transfer at molecule-metal interfaces. *Chem. Rev.* **2006**, *106*, 4281–4300.

(65) Fukui, K.; Tanaka, K. Distance dependence of photoinduced electron transfer in DNA. *Angew. Chemie, Int. Ed.* **1998**, *37*, 158–161.

(66) de Silva, a P.; Moody, T. S.; Wright, G. D. Fluorescent PET (photoinduced electron transfer) sensors as potent analytical tools. *Analyst* **2009**, *134*, 2385–2393.

(67) Bissell, R.; Prasanna de Silva, A.; Nimal Gunaratne, H. Q.; Mark Lynch, P. L.; Maguire, G. M.; McCoy, C.; Samankumara Sandanayake, K. R. A. Fluorescent PET (photoinduced electron transfer) sensors. In *Photoinduced Electron Transfer*; 1993; Vol. 168, pp. 223–264.

(68) Piotrowiak, P. Photoinduced electron transfer in molecular systems: recent developments. *Chem. Soc. Rev.* **1999**, *28*, 143–150.

(69) Tobin, P. H.; Wilson, C. J. Examining photoinduced energy transfer in pseudomonas aeruginosa azurin. *J. Am. Chem. Soc.* **2014**, *136*, 1793–1802.

(70) Jin, Qusheng, C. M. B. Kinetics of Electron Transfer through the Respiratory Chain. *Biophys. J.* **2002**, *83*, 1797–1808.

(71) Schertl P, B. H. Respiratory electron transfer pathways in plant mitochondria. *Front. Plant Sci.* **2014**, *5*, 1–11.

(72) G.F. Moore, G. W. B. Energy Conversion in Photosynthesis: A Paragigm for Solar Fuel Production. *Annu. Rev. Condens. Matter Phys.* **2011**, *2*, 303–327.

(73) B.E. Ramirez, H. B. G. The currents of life: the terminal electron-transfer complex of respiration. *Proc. Natl. Acad. Sci. U. S. A.* **1995**, *92*, 11949–11954.

(74) Jonkheijm P, Weinrich D, Schröder H, Niemeyer CM, W. H. Chemical strategies for generating protein biochips. *Angew Chem Int Ed Engl.* **2008**, *47*, 9618–47.

(75) Rehm, D.; Weller, A. Kinetics of fluorescence quenching by electron and hydrogen-atom transfer. *Isr. J. Chem.* **1970**, *8*, 259–271.

(76) Stuchebrukhov, A. Long-distance electron tunneling in proteins. *Theor. Chem. Acc.* **2003**, *110*, 291–306.

(77) Gray, H. B.; Winkler, J. R. Long-range electron transfer. *Proc. Natl. Acad. Sci. U. S. A.* **2005**, *102*, 3534–9.

(78) Winkler, J. R. J. R. Electron tunneling pathways in proteins. *Curr. Opin. Chem. Biol.* **2000**, *4*, 192–198.

(79) Wenger, O. S. Barrier heights in long-range electron tunneling. *Inorganica Chim. Acta* **2011**, *374*, 3–9.

(80) Jochen Blumberger Recent Advances in the Theory and Molecular Simulation of Biological Electron Transfer Reactions. *Chem. Rev.* **2015**, *115*, 11191–11238.

(81) Steinberg, I. Z. Long-range nonradiative transfer of electronic excitation energy in proteins and polypeptides. *Annu. Rev. Biochem.* **1971**, *40*, 83–114.

(82) Gray, H. B.; Winkler, J. R. Long-range electron transfer. *Proc. Natl. Acad. Sci. U. S. A.* **2005**, *102*, 3534–3539.

(83) Winkler, J. R.; Gray, H. B. Long-range electron tunneling. *J. Am. Chem. Soc.* **2014**, *136*, 2930–2939.

(84) Voityuk, A. a. Long-range electron transfer in biomolecules. Tunneling or hopping? *J. Phys. Chem. B* **2011**, *115*, 12202–12207.

(85) Kriegl, J. M.; Nienhaus, G. U. Structural, dynamic, and energetic aspects of long-range electron transfer in photosynthetic reaction centers. *Proc. Natl. Acad. Sci. U. S. A.* **2004**, *101*, 123–8.

(86) Schlag EW, Sheu SY, Yang DY, Selzle HL, L. S. Distal charge transport in peptides. *Angew Chem Int Ed Engl.* **2007**, *46*, 3196–3210.

(87) Crane BR, Di Bilio AJ, Winkler JR, G. H. Electron tunneling in single crystals of Pseudomonas aeruginosa azurins. *J. Am. Chem. Soc.* **2001**, *123*, 11623–11631.

(88) Chang I J, Gray H B, W. J. R. High-driving-force electron transfer in metalloproteins: intramolecular oxidation of ferrocytochrome c by Ru(2,2'-bpy)2(im)(his-33)3+. *J. Am. Chem. Soc.* **1991**, *113*, 7056–7057.

(89) Farver, O.; Pecht, I. Long-range intramolecular electron transfer in azurins. *Proc. Natl. Acad. Sci. U. S. A.* **1989**, *86*, 6968–72.

(90) Farver, O.; Jeuken, L. J. C.; Canters, G. W.; Pecht, I. Role of ligand substitution on long-range electron transfer in azurins. *Eur. J. Biochem.* **2000**, *267*, 3123–3129.

(91) Farver, O.; Skov, L. K.; Van De Kamp, M.; Canters, G. W.; Pecht, I. The effect of driving force on intramolecular electron transfer in proteins. Studies on single-site mutated azurins. *Eur. J. Biochem.* **1992**, *210*, 399–403.

(92) Farver, O.; Skov, L. K.; Pascher, T.; Karlsson, B. G.; Nordling, M.; Lundberg, L. G.; Vänngård, T.; Pecht, I. Intramolecular electron transfer in single-site-mutated azurins. *Biochemistry* **1993**, *32*, 7317–7322.

(93) Istvan Szundi , Jenny A. Cappuccio , Natalia Borovok, A. B. K. Photoinduced Electron Transfer in the Cytochrome c/Cytochrome c Oxidase Complex Using Thiouredopyrenetrisulfonate-Labeled Cytochrome c. Optical Multichannel Detection. *Biochemistry* **2001**, *40*, 2186–2193.

(94) Alexander B. Kotlyar , Natalia Borovok, M. H. Photoinduced Electron Transfer in Singly Labeled Thiouredopyrenetrisulfonate Cytochrome c Derivatives. *Biochemistry* **1997**, *36*, 15828–15833.

(95) Kotlyar, A.; Borovok, N.; Hazani, M.; Szundi, I.; Einarsdóttir, Ó. Photoinduced intracomplex electron transfer between cytochrome c oxidase and TUPS-modified cytochrome c. *Eur. J. Biochem.* **2000**, *267*, 5805–5809.

(96) Alagaratnam, S.; Meeuwenoord, N. J.; Navarro, J.; Hervás, M.; De la Rosa, M.; Hoffmann, M.; Einsle, O.; Ubbink, M.; Canters, G. W. Probing the reactivity of different forms of azurin by flavin photoreduction. *FEBS J.* **2011**, *278*, 1506–21.

(97) Martínez-Junza, V.; Rizzi, A. C.; Alagaratnam, S.; Bell, T. D. M.; Canters, G. W.; Braslavsky, S. E. Flavodoxin relaxes in microseconds upon excitation of the flavin chromophore: detection of a UV-visible silent intermediate by laser photocalorimetry. *Photochem. Photobiol.* **2009**, *85*, 107–10.

(98) Alagaratnam, S. *Electron Transfer in Flavodoxin-based Redox Maquettes*; Institute of Chemistry, Faculty of Mathematics & Natural Sciences, Leiden University, 2005.

(99) Crystal Shih, Anna Katrine Museth, Malin Abrahamsson, Ana Maria Blanco-Rodriguez, Angel J. Di Bilio, Jawahar Sudhamsu, Brian R. Crane, Kate L. Ronayne, Mike Towrie, Antonín Vlček Jr., John H. Richards, Jay R. Winkler, and H. B. G. Tryptophan-Accelerated Electron Flow Through Proteins. *Science (80-.).* **2008**, *320*, 1760–1762.

(100) Warren, J. J.; Herrera, N.; Hill, M. G.; Winkler, J. R.; Gray, H. B. Electron flow through nitrotyrosinate in Pseudomonas aeruginosa azurin. *J. Am. Chem. Soc.* **2013**, *135*, 11151–11158.

(101) Winkler JR, G. H. Could tyrosine and tryptophan serve multiple roles in biological redox

processes? *Philos. Trans. A Math. Phys. Eng. Sci.* **2015**, *373*, 2037.

(102) Farver, O.; Zhang, J.; Chi, Q.; Pecht, I.; Ulstrup, J. Deuterium isotope effect on the intramolecular electron transfer in Pseudomonas aeruginosa azurin. *Proc. Natl. Acad. Sci. U. S. A.* **2001**, *98*, 4426–4430.

(103) Warren JJ, Shafaat OS, Winkler JR, G. H. Proton-coupled electron hopping in Ru-modified P. aeruginosa azurin. *J. Biol. Inorg. Chem.* **2016**, *21*, 113–119.

(104) Winkler JR, G. H. Electron flow through biological molecules: does hole hopping protect proteins from oxidative damage? *Q. Rev. Biophys.* **2015**, *48*, 411–420.

(105) Jensen, P. S.; Chi, Q.; Zhang, J.; Ulstrup, J. Long-Range interfacial electrochemical electron transfer of Pseudomonas aeruginosa azurin-gold nanoparticle hybrid systems. *J. Phys. Chem. C* **2009**, *113*, 13993–14000.

(106) Chin, Q.; Zhang, J.; Nielsen, J. U.; Friis, E. P.; Chorkendorff, I.; Canters, G. W.; Andersen, J. E. T.; Ulstrup, J. Molecular monolayers and interfacial electron transfer of Pseudomonas aeruginosa azurin on Au(111). *J. Am. Chem. Soc.* **2000**, *122*, 4047–4055.

(107) Chi, Q.; Zhang, J.; Andersen, J. E. T.; Ulstrup, J. Ordered assembly and controlled electron transfer of the blue copper protein azurin at gold (111) single-crystal substrates. *J. Phys. Chem. B* **2001**, *105*, 4669–4679.

(108) Friis, E. P.; Andersen, J. E. T.; Madsen, L. L.; Møller, P.; Ulstrup, J. In situ STM and AFM of the copper protein Pseudomonas aeruginosa azurin. *J. Electroanal. Chem.* **1997**, *431*, 35–38.

(109) Beratan, D.; Betts, J.; Onuchic, J. Protein electron transfer rates set by the bridging secondary and tertiary structure. *Science (80-.).* **1991**, *252*, 1285–1288.